Title	Electrochemical behavior of hexafluoroniobate, heptafluorotungstate, and oxotetrafluorovanadate anions in N-butyl-N-methylpyrrolidinium bis(trifluoromethylsulfonyl)amide room temperature ionic liquid
Author(s)	Kanatani, Takatsugu; Matsumoto, Kazuhiko; Nohira, Toshiyuki; Hagiwara, Rika
Citation	Journal of Fluorine Chemistry (2011), 132(10): 673-678
Issue Date	2011-10
URL	http://hdl.handle.net/2433/148613
Right	© 2011 Elsevier B.V.
Type	Journal Article
Textversion	author

Electrochemical behavior of hexafluoroniobate, heptafluorotungstate, and oxotetrafluorovanadate anions in *N*-butyl-*N*-methylpyrrolidinium bis(trifluoromethylsulfonyl)amide room temperature ionic liquid

Takatsugu Kanatani, Kazuhiko Matsumoto, Toshiyuki Nohira, Rika Hagiwara*

Graduate School of Energy Science, Kyoto University, Yoshida, Sakyo-ku, Kyoto 606-8501, Japan

*E-mail: hagiwara@energy.kyoto-u.ac.jp, Tel: +81-75-753-5822, Fax: +81-75-753-5906

Keywords: Ionic liquids, NbF_6^-, WF_7^-, VOF_4^-, Diffusion coefficient, Stokes radius

†Dedicated to Prof. Alain Tressaud on the occasion of receiving the ACS award for Creative Work in Fluorine Chemistry.

Abstract

Electrochemical behavior of hexafluoroniobate ($Nb(V)F_6^-$), heptafluorotungstate ($W(VI)F_7^-$), and oxotetrafluorovanadate ($V(V)OF_4^-$) anions has been investigated in *N*-butyl-*N*-methylpyrrolidinium bis(trifluoromethylsulfonyl)amide (BMPyrTFSA) ionic liquid at 298 K by means of cyclic voltammetry and chronoamperometry. Cyclic voltammograms at a Pt electrode showed that $Nb(V)F_6^-$ anion is reduced to $Nb(IV)F_6^{2-}$ by a one-electron reversible reaction. Electrochemical reductions of $W(VI)F_7^-$ and $V(V)OF_4^-$ anions at a Pt electrode are quasi-reversible and irreversible reactions, respectively, according to cyclic voltammetry. The diffusion coefficients of $Nb(V)F_6^-$, $W(VI)F_7^-$ and $V(V)OF_4^-$ determined by chronoamperometry are 1.34×10^{-7}, 7.45×10^{-8} and 2.49×10^{-7} $cm^2\ s^{-1}$, respectively. The Stokes radii of $Nb(V)F_6^-$, $W(VI)F_7^-$, and $V(V)OF_4^-$ in BMPyrTFSA have been are calculated to be 0.23, 0.38, and 0.12 nm, from the diffusion coefficients and viscosities obtained.

1. Introduction

Electrochemistry of transition metal species in ionic liquids (ILs) has been widely investigated due to the wider electrochemical windows of ILs than those of aqueous systems in addition to their unique properties such as low melting points, nonflammability, low vapor pressure, and wide temperature range of liquid phase [1–9]. The electrochemical behavior of Fe(II) [10, 11], Co(II) [12], Ti(IV) [2, 13], V(III), V(IV), V(V), [14], Mg(II), U(IV), Ta(V), Mn(II), Ru(III), and Rh(III) [13] in ILs was reported in view of the application for metal electrodeposition. Redox behavior of some transition metals, such as Fe(II), Sm(III), Eu(III), and Yb(III) in BMPyrTFSA (*N*-butyl-*N*-methylpyrrolidinium bis(trifluoromethylsulfonyl)amide) was investigated for redox flow batteries using ILs [15].

A series of *N*-alkyl-*N*-methylpyrrolidinium salts based on the fluorocomplex anions (BF_4^-, PF_6^-, NbF_6^-, TaF_6^-, and WF_7^-) have been prepared by fluoroacid-base reactions between fluorohydrogenate ILs and binary fluoroacid (AF_m), and have been characterized by spectroscopic, physical, and chemical methods [16]. Although electrochemical data are available for some chloro- and bromo-metallate anions [17-23], there are not many reports on electrochemical data for fluorometallate and oxofluorometallate anions and, to our knowledge, no reports are available for the electrochemical behavior of $Nb(V)F_6^-$, $W(VI)F_7^-$, and $V(V)OF_4^-$ at 298 K. In this paper, the electrochemical behavior of $Nb(V)F_6^-$, $W(VI)F_7^-$, and $V(V)OF_4^-$ in BMPyrTFSA at 298 K is discussed in detail, where BMPyrTFSA was chosen as a medium because of its high electrochemical stability and easy handling.

2. Results and discussion

2.1. Electrochemical behavior of $Nb(V)F_6^-$

Figure 1 shows the cyclic voltammograms at a Pt electrode in BMPyrTFSA containing 29.2 mM $BMPyrNbF_6$. Only one cathodic wave is observed around –2.2 V vs. Ag^+/Ag during the cathodic scan. The cathodic and anodic peak current densities (i_p^c and i_p^a) increase with increase in scan rate, and their peak potentials (E_p^c) are essentially unchanged, indicating a high reversibility of this electrochemical reaction. In the case of a reversible reaction, the following relation holds [24]:

$$\left|E_p^c - E_{p/2}^c\right| = \frac{0.0565}{n} \quad (1)$$

where $E_{p/2}^c$ is the half-peak potential and *n* is the number of electrons. The value of *n* is calculated to be around 0.8, suggesting the number of electrons for this reaction is one. Thus, the present electrode reaction of NbF_6^- in BMPyrTFSA is described as follows:

$$Nb(V)F_6^- + e^- \rightarrow Nb(IV)F_6^{2-} \quad (2)$$

Table S1 lists the data of cyclic voltammogram obtained for the reduction of NbF_6^-. As shown in Figure 2, the linear dependence of the cathodic peak current density (i_p^c) and square root of scan rate ($v^{1/2}$) also confirms the electrochemical reduction of NbF_6^- is a reversible reaction. The diffusion coefficient of NbF_6^- is calculated from the slope of Figure 2 using Eq. (3) [24]:

$$i_p^c = \left(2.69 \times 10^5\right) n^{3/2} D^{1/2} C v^{1/2} \quad (3)$$

where *C* is the concentration of NbF_6^- and *D* is the diffusion coefficient. From this equation, *D* was calculated to be 1.46×10^{-7} cm^2 s^{-1}.

The electrochemical behavior of NbF_6^- was also investigated by chronoamperometry. Figure 3 shows the Cottrell plot for the reduction reaction from NbF_6^- to NbF_6^{2-} at a Pt electrode, where the potential was stepped from –0.6 to –2.3 V vs. Ag^+/Ag. The Cottrell equation describing the current density(i) against time (t) for the reduction of electroactive species is given by Eq. (4) [24].

$$i = nFCD^{1/2}\pi^{-1/2}t^{-1/2} \quad (4)$$

The obtained straight line passing through the origin in Figure 3 indicates the validity of a simple diffusion controlled reduction, and enables determination of the diffusion coefficient of NbF_6^-. The obtained value of 1.34 $\times$ 10^{-7} cm^2 s^{-1} is close to that obtained from cyclic voltammetry. In the 44.4% $AlCl_3$–55.6% EMImCl ionic liquid at 313 K, the diffusion coefficient of $NbCl_6^-$ was reported as 4.98 $\times$ 10^{-7} cm^2 s^{-1} [25]. This value is higher than that of NbF_6^- in the present study, which is probably due to the lower viscosity of the 44.4%$AlCl_3$ – 55.6%EMImCl ionic liquid (21 cP at 313 K) [26] than that of the BMPyrTFSA ionic liquid (72 cP at 298 K).

2.2. Electrochemical behavior of W(VI)F_7^-

Figure 4 shows the cyclic voltammograms of a Pt electrode in BMPyrTFSA containing 61.8 mM of $BMPyrWF_7$. The peak potential of the cathodic wave shifts to the negative potential with increase in scan rate from 1 to 20 mV s^{-1}, suggesting that this is not a reversible reaction. If the reaction is totally irreversible, $E_p^c - E_{p/2}^c$ is independent on scan rate [24], whereas the value of $E_p^c - E_{p/2}^c$ increases with increase of scan rate. Thus, the present reaction is considered to be a quasi-reversible one. Table S2 lists the voltammetric parameters obtained for WF_7^-. According to the previous report on electrochemical behavior of WCl_6^- in the

basic $AlCl_3$-EMImCl ionic liquid containing $KWCl_6$ (or WCl_6) [27], WCl_6^- is reduced to WCl_6^{2-} via a one-electron reaction at 0.45 V vs. Al^{3+}/Al in 66.7%$AlCl_3$-33.3%EMImCl melt. This suggests that the reduction from W(V) to W(IV) in the present system occurs at a more negative potential than –1.0 V vs Ag^+/Ag and the reduction current observed around –1.0 V vs Ag^+/Ag in Figure 4 is probably assigned to the following reduction reaction.:

$$W(VI)F_7^- + e^- \rightarrow W(V)F_7^{2-} \quad (5)$$

In order to estimate the diffusion coefficient of WF_7^-, chronoamperometry was performed at a Pt electrode. Figure 5 shows the Cottrell plot, where the potential was stepped from –0.8 to –1.5 V vs. Ag^+/Ag. The linearity and zero-intercept of the plot indicates the validity of a simple diffusion controlled reaction. The value of D_R is calculated to be 7.45×10^{-8} cm^2 s^{-1} at 298 K with n = 1. The diffusion coefficients of some chlorotungstate anions, WCl_6^-, WCl_6^{2-} and $W_2Cl_9^{3-}$, in basic 44.4 mol% $AlCl_3$– 55.6% EMImCl ionic liquid at 313 K (21 cP) were reported to be $(2.8 \pm 0.2)\times10^{-7}$, $(2.2 \pm 0.1)\times10^{-7}$ and $(1.5 \pm 0.1)\times10^{-7}$ cm^2 s^{-1}, respectively [27]. These values for chlorotungstate anions are larger than that of WF_7^- in BMPyrTFSA at 298 K (76 cP), which is again explained by the difference in the viscosity of the two ionic liquids.

2.3. Electrochemical behavior of $V(V)OF_4^-$

The new salt, $BMPyrVOF_4$, is a pale-yellow solid at room temperature. Differential scanning calorimetry (DSC) revealed that its melting point is 323 K. According to the previous study on the crystal structures of $CsVOF_4$ [28] and $EMImVOF_4$[29], VOF_4^- is not a discrete anion in the solid state but forms the polymeric or

oligomeric unit (the $(VOF_4^-)_n$ chain in $CsVOF_4$ and $(VOF_4^-)_2$ dimer in $EMImVOF_4$) via a weak V···F interaction. Figure 6 shows Raman spectra of (a) $BMPyrVOF_4$ (solid), (b) 1.53 M $BMPyrVOF_4$ in BMPyrTFSA (liquid), and (c) BMPyrTFSA (liquid). The vibrational frequency of 1005 cm^{-1} in the Raman spectrum of $BMPyrVOF_4$ is assigned to the V=O stretching mode and is similar to that observed for $EMImVOF_4$ (1012 cm^{-1} in Raman spectrum), suggesting VOF_4^- forms a oligomeric unit as observed in the previous study [29]. The Raman spectrum (a) in Figure 6 shows two peaks in this region. The vibrational mode at 1005 cm^{-1} can be assigned to the V=O stretching in $(VOF_4^-)_2$ due to the similarity in frequency. The vibrational mode at 1027 cm^{-1} corresponds to the stronger V=O bond than that in $(VOF_4^-)_2$ caused by the break of the dimeric anion. Although the Raman spectrum of the electrolyte used in the present study (17.0 mM $BMPyrVOF_4$ in BMPyTFSA), unfortunately, does not show a clear peak assigned to the V=O stretching mode because of its low concentration, the break of the polymeric VOF_4^- is highly possible in this diluted electrolyte.

Figure 7 shows cyclic voltammograms of a Pt electrode in BMPyrTFSA containing 17.0 mM of $BMPyrVOF_4$. Table S3 lists the voltammetric parameters obtained for VOF_4^-. The previous report mentioned that the one-electron reduction of V(V) species to V(IV) species was observed around 0.4 V vs. Al^{3+}/Al in 50%$AlCl_3$-50%EMImCl at 298 K [14]. Thus, the most probable reaction for the reduction wave around –1.0 V in Figure 7 is:

$$V(V)OF_4^- + e^- \rightarrow V(IV)OF_4^{2-} \quad (6)$$

E_p^c shifts to the negative potential with increase in scan rate. Figure 8 shows the $\ln v^{1/2} - E_p^c$ plot for the reduction of VOF_4^-. The linear relationship between $\ln v^{1/2}$ and E_p^c indicates that this reaction is totally

irreversible as is given by Eq. (7) [24]:

$$E_{\mathrm{p}}^{\mathrm{c}} = E^{0'} - \frac{RT}{\alpha n_{\alpha} F}\left[0.780 + \ln\left(\frac{D^{1/2}}{k^{0}}\right) + \ln\left(\frac{\alpha n_{a} F v}{RT}\right)^{1/2}\right] \tag{7}$$

where $E^{0'}$ is the standard formal potential of the redox couple, R is the gas constant, T is the temperature, α is the transfer coefficient, n_{α} is the number of electrons involved in the rate determining step, F is the Faraday constant, and k^0 is the standard heterogeneous rate constant. The product, αn_{α} is estimated from Eq. (8) [24]:

$$\left|E_{\mathrm{p}}^{\mathrm{c}} - E_{\mathrm{p/2}}^{\mathrm{c}}\right| = \frac{47.7}{\alpha n_{\alpha}} \tag{8}$$

The value of αn_{α} is estimated to be 0.49 at the scan rate of 0.1 mV s^{-1}, which suggests the number of electrons transferred in the rate determining step is one, where α is assumed to be 0.5. The $v^{1/2}$–$i_{\mathrm{p}}^{\mathrm{c}}$ plot shown in Figure 9 confirms the linear relationship between them, and allows the determination of the diffusion coefficient from the slope by Eq. (9) [24]:

$$i_{\mathrm{p}}^{\mathrm{c}} = \left(2.99 \times 10^{5}\right) n\left(\alpha n_{\alpha}\right)^{1/2} D^{1/2} C v^{1/2} \tag{9}$$

The obtained diffusion coefficient of VOF_4^- is 2.81×10^{-7} cm^2 s^{-1} at 298 K.

Chronoamperometry was also performed using a Pt electrode to determine the diffusion coefficient of VOF_4^-. Figure 10 shows the $t^{-1/2}$ - i plot in the case that the electrode potential was stepped to –1.2 V vs. Ag^+/Ag. The linearity and zero-intercept obtained from the plot indicate that the Cottrell equation (Eq. 4) holds in the present case. The diffusion coefficient is determined to be 2.49×10^{-7} cm^2 s^{-1} at 298 K, which is the similar value obtained by voltammetry. According to the previous study [30], the diffusion coefficients of $V(II)_{solv.}$ in acidic 66.7 mol% $AlCl_3$–33.3% EMImCl ionic liquid at 353 K is 2.41×10^{-7} cm^2 s^{-1}. This value is similar to that

of VOF_4^- in BMPyrTFSA, although the viscosity of 66.7% $AlCl_3$–33.3% EMImCl at 353 K (4.8 cP) is much lower than that of BMPyrTFSA (74 cP). Difference in the coordination environment around metal species may lead to this coincidence.

2.4 Stokes radius of the diffusion species

The Stokes – Einstein equation given in Eq. (10) is applied to NbF_6^-, WF_7^-, and VOF_4^- in the BMPyrTFSA ionic liquid system:

$$r_s = \frac{kT}{6\pi\eta D} \tag{10}$$

where r_s is the Stokes radius, η is the viscosity, and k is the Boltzmann constant. For this purpose, viscosities of BMPyrTFSA containing 29.2 mM $BMPyrNbF_6$, 61.8 mM of $BMPyrWF_7$, or 17.0 mM of $BMPyrVOF_4$ were measured (72, 76, or 74 cP, respectively). Table 1 lists the calculated Stokes radii of NbF_6^-, WF_7^-, and VOF_4^- [26-28]. The Stokes radii for several related chloro-complex anions in *N*$AlCl_3$–(1–*N*)EMImCl (*N* = 44.4, 49.0, and 66.7%) are also listed for comparison [30]. The Stokes radii of NbF_6^- (0.22 nm) in BMPyrTFSA and $NbCl_6^-$ (0.21 nm) in 49.0%$AlCl_3$-51.0%EMImCl are close to each other. Although the size of NbF_6^- determined in a crystal structure (Nb–F bond length: ~0.188 nm [31-33]) is smaller than that of $NbCl_6^-$ (Nb–Cl bond length: ~0.235 nm [34]), the difference in cation-anion interactions, namely, the form of the ion pair or ion aggregate, and the difference in temperature probably influence the r_s values. The Stokes radius of WF_7^- (0.38 nm) is similar to that of WCl_6^- (0.38 nm), and smaller than that of WCl_6^{2-} (0.49 nm). It should be noted that the r_s value for WF_7^- (0.38 nm) is significantly larger than that for NbF_6^- (0.22 nm), even taking into account the larger ion

size of WF_7^- than that of NbF_6^- [35]. This suggests that these species diffuse in a totally different form in BMPyrTFSA. The similar case was also seen for $NbCl_6^-$ and WCl_6^-[27, 29]. The r_s of VOF_4^- anion was calculated to be relatively small value of 0.12 nm. The small r_s size is explained by the weak interactions between VOF_4^- anion and solvent, which results in the large diffusion coefficient of VOF_4^-. The order of the Stokes radii of the anionic species obtained in this study follows the order of their ionic radii of the central atom (V(V) (0.060 nm) < Nb(V) (0.078 nm) < W(VI) (0.087 nm))[36] although the coordination number and ligands (O or F) are different within the three species.

3. Conclusions

Electrochemical behaviors of NbF_6^-, WF_7^-, and VOF_4^- were studied in *N*-butyl-*N*-methylpyrrolidinium bis(trifluoromethylsulfonyl)amide (BMPyrTFSA) ionic liquid at 298 K by cyclic voltammetry and chronoamperometry. Reduction of NbF_6^- at a Pt electrode proceeds via a one-electron reversible process, suggesting that the product to NbF_6^{2-}. The diffusion coefficient of NbF_6^- is determined to be 1.34×10^{-7} cm^2 s^{-1}. The reduction of WF_7^- at a Pt electrode is a quasi-reversible process to WF_7^{2-}. The diffusion coefficient of WF_7^- is calculated to be 7.45×10^{-8} cm^2 s^{-1}. The reduction of VOF_4^- at a Pt electrode is an irreversible process to VOF_4^{2-} with the αn_α value of 0.49. The diffusion coefficient of VOF_4^- is calculated to be 2.49×10^{-7} cm^2 s^{-1}. From the Stokes-Einstein equation, the Stokes radii of NbF_6^-, WF_7^-, and VOF_4^- are estimated to be 0.22, 0.38, and 0.12 nm, respectively. The significant difference in size suggests the different coordination environments around them.

4. Experimental

4.1 General

Nonvolatile materials were handled under a dry and deoxygenated Ar atmosphere in a glove box. The fluorocomplex salts, $BMPyrNbF_6$ and $BMPyrWF_7$, were synthesized by the reactions of *N*-butyl-*N*-methylpyrrolidinium fluorohydrogenate IL, $BMPyr(FH)_{2.3}F$, and Lewis acid fluorides (NbF_5 (Aldrich, purity 99 %) and WF_6 (Central Glass, purity 99.999 %)) according to the literature [16]. The room temperature ionic liquid, BMPyrTFSA (Kanto Kagaku), was dried under vacuum at 373 K for two days. The fluorometallate and oxofluorometallate sources were weighed and added to BMPyrTFSA, followed by agitation overnight. Electrochemical measurements were carried out in a PFA (tetrafluoroethylene-perfluoroalkylvinylether copolymer) cell (~2 mL) under the Ar atmosphere at 298 K with the aid of an electrochemical measurement system HZ-3000 (Hokuto Denko). The materials for working and counter electrodes were a Pt plate (0.18 cm^2) and a glassy carbon rod (0.36 cm^2), respectively. The reference electrode was made of a silver wire immersed in $EMImBF_4$ containing 0.05 M $AgBF_4$ separated from the electrolyte by a PTFE filter. The typical resistance of the electrolyte was ca..100 Ω and the resulting ohmic drop was negligible because of the small area of the working electrode. Viscosity was measured by a cone-plate rheometer DV-II + Pro (Brookfield Engineering Laboratories Inc.).

4.2 Synthesis of $BMPyrVOF_4$

The VOF_4^- source, $BMPyrVOF_4$, was prepared in the following manner. [25]. Vanadium oxide

trifluoride (Aldrich, purity 99 %, 0.53 g (4.28 mmol)) loaded in one arm of a T-shaped PFA was slowly added onto $BMPyr(FH)_{2.3}F$ (4.28 mmol) in the other arm at room temperature. After the addition of VOF_3, the obtained liquid was stirred for 5 hours. A pale-yellow powder sample was obtained after removal of liberated HF under dynamic vacuum at 340 K. Vibrational spectroscopy and elemental analysis identified the solid as $BMPyrVOF_4$. Anal. Calcd. for $C_9H_{20}N_1V_1O_1F_4$: C, 37.90; H, 7.07; N, 4.91. Found: C, 37.86; H, 7.05; N, 4.93. Raman (solid) for VOF_4^- (frequency / cm^{-1} (Relative intensity): 1005(m), 628(m), 345(s), 318(w), 242(m), and 234(m); IR for VOF_4^- (frequency / cm^{-1} (Relative intensity): 999(m), 632(s), and 590(s), where s, m and w for relative intensity denote strong, medium and weak, respectively.

References

[1] J. S. Wilkes, J.A. Levisky, R.A. Wilson, C.L. Hussey, Inorg. Chem. 21 (1982) 1263-1264.

[2] I. W. Sun, J.R. Sanders, C.L. Hussey, J. Electrochem. Soc. 136 (1989) 1415-1419.

[3] R. T. Carlin, R.A. Osteryoung, J.S. Wilkes, J. Rovang, Inorg. Chem. 29 (1990) 3003-3009.

[4] T. Tsuda, C.L. Hussey, G.R. Stafford, J.E. Bonevich, J. Electrochem. Soc. 150 (2003) C234-C243.

[5] I. Mukhopadhyay, C.L. Aravinda, D. Borissov, W. Freyland, Electrochim. Acta 50 (2005) 1275-1281.

[6] Y. Katayama, K. Ogawa, T. Miura, Electrochemistry 73 (2005) 576-578.

[7] H. Ohno, Editor, *Electrochemical Aspects of Ionic Liquids*, John Wiley & Sons, New Jersey (2005).

[8] S. Zein El Abedin, F. Endres, Chemphyschem. 7 (2006) 58-61.

[9] S. Zein El Abedin, E.M. Moustafa, R. Hempelmann, H. Natter, F. Endres, Chem. Phys. Chem. 7 (2006) 1535-1543.

[10] M. Yamagata, N. Tachikawa, Y. Katayama, T. Miura, Electrochim. Acta 52 (2007) 3317-3322.

[11] C. Nanjundiah, K. Shimizu, R.A. Osteryoung, J. Electrochem. Soc. 129 (1982) 2474-2480.

[12] R. Fukui, Y. Katayama, T. Miura, Electrochemistry 73 (2005) 567-569.

[13] W. Simka, D. Puszczyk, G.. Nawrat, Electrochim. Acta 54 (2009) 5307-5319.

[14] D.M. Ryan, T.L. Riechel, T. Welton, J. Electrochem. Soc. 149 (2002) A371-A378.

[15] M. Yamagata, Y. Katayama, T. Miura, J. Electrochem. Soc. 153 (2006) E5-E9.

[16] T. Kanatani, R. Ueno, T. Nohira, R. Hagiwara, J. Fluorine Chem. 130 (2009) 979-984.

[17] Q. Zhiyu, T. Pierre, J. Appl. Electrochem. 15 (1985) 259-265.

[18] S. Senderoff, G. W. Mellors, J. Electrochem. Soc. 113 (1966) 66-71.

[19] V.I. Konstantiov, E.G. Polyakov, P.T. Stangrit, Electrochim. Acta 26 (1979) 445-448.

[20] F. Matthiesen, E. Chrstensen, J.H. von Barner, N.J. Bjerrum, J. Electrochem. Soc. 143 (1996) 1793-1799.

[21] V. Van, A. Silný, J. Híveš, V. Daněk, Electrochem. Commum. 1 (1999) 295-300.

[22] C. Rosenkilde, A. Vik, T. Østvold, E. Chritensen, N. Bjerrum, J. Electrochem. Soc. 147 (2000) 3790-3800.

[23] U. Stöhr, W. Freyland, Electrochim. Acta 44 (1999) 2199-2207.

[24] A. J. Bard, L.R. Faulkner, Electrochemical Methods, 2nd ed.; John Wiley & Sons; New York, 2001.

[25] I-Wen Sun, C.L. Hussey, Inorg. Chem. 28 (1989) 2731-2737.

[26] A.A. Fannin, D.A. Floreani, L.A. King, J.S. Landers, B.J. Piersma, D.J. Stech, R.L. Vaughn, J.S. Wilkes, J.L. Williams, J. Phys. Chem. 88 (1984) 2614-2621.

[27] T.B. Scheffler, C.L. Hussey, Inorg. Chem. 23 (1984) 1926-1932.

[28] G. W. Bushnell , K. C. Moss , Can. J. Chem. 50 (1972) 3700-3705.

[29] T. Kanatani, K. Matsumoto, R. Hagiwara, Eur. J. Inorg. Chem. (2010) 1049-1055.

[30] T. Tsuda and C.L. Hussey, J. Min. Met. 39 (2003) 3-22.

[31] R.W. Berg, Coord. Chem. Rev. 113 (1992) 1-130.

[32] M.B. de Bournoniville, B. Bizot, J. Chassaing, M. Quarton, J. Solid State Chem. 62 (1986) 212-219.

[33] K. Matsumoto, R. Hagiwara, Z. Mazej, P. Benkič, B. Žemva, Solid State Sci. 8 (2006) 1250-1257.

[34] A. Hagebach, J. Strähle, Z. Anorg. Allg. Chem. 627 (2001) 726-730.

[35] S. Giese, K. Seppelt, Angew. Chem., Int. Ed. Engl. 33, (1994) 461-463.

[36] R. D. Shannon, Acta Cryst. A32 (1976) 751-767. The radius of seven-coordinated Mo(IV) is used for seven-coordinated W(IV).

Table 1 The diffusion coefficient (D, obtained by chronoamperometry) and Stokes radius (r_s) of NbF_6^-, WF_7^-, and VOF_4^- in BMPyrTFSA and of related species in a chloroaluminate ionic liquid. The viscosities (η) of the systems are also listed.

Species	System	Temperature / K	$10^8 D$ / cm^2 s^{-1}	η / cP	r_s / nm	Reference
$Nb(V)F_6^-$	BMPyrTFSA	298	13.4	72	0.22	This work
$Nb(V)Cl_6^-$	49.0% $AlCl_3$-51.0%EMImCl	313	82.1	13	0.21	[25, 26]
$Nb(V)Cl_6^-$	44.4% $AlCl_3$-55.6%EMImCl	313	49.8	21	0.22	[25, 26]
$W(VI)F_7^-$	BMPyrTFSA	298	7.45	76	0.38	This work
$W(V)Cl_6^-$	44.4% $AlCl_3$-55.6%EMImCl	313	28	–	0.38	[26, 27]
$W(IV)Cl_6^{2-}$	44.4% $AlCl_3$-55.6%EMImCl	313	22	–	0.49	[26, 27]
$V(V)OF_4^-$	BMPyrTFSA	298	24.9	74	0.12	This work
$V(II)_{solv}$	66.7% $AlCl_3$-33.3%EMImCl	353	24.1	4.8	2.22	[30]

Figure captions

Figure 1 Cyclic voltammograms of a Pt electrode in BMPyrTFSA containing 29.2 mM of $BMPyrNbF_6$ at 298 K. Scan rate: (a) 1, (b) 2, (c) 5, (d) 10, and (e) 20 mV s^{-1}.

Figure 2 The $v^{1/2} - i_p^c$ plots for the reduction of NbF_6^- in BMPyrTFSA containing 29.2 mM of $BMPyrNbF_6$. .

Figure 3 The $t^{-1/2} - i$ plots for the reduction of NbF_6^- in BMPyrTFSA containing 29.2 mM of $BMPyrNbF_6$.

Figure 4 Cyclic voltammograms of a Pt electrode in BMPyrTFSA containing 61.8 mM of $BMPyrWF_7$ at 298 K. Scan rate: (a) 1, (b) 2, (c) 5, (d) 10, and (e) 20 mV s^{-1}.

Figure 5 The $t^{-1/2} - i$ plots for the reduction of WF_7^- in BMPyrTFSA containing 61.8 mM of $BMPyrWF_7$.

Figure 6 Raman spectra of (a) $BMPyrVOF_4$ (solid), (b) BMPyrTFSA containing 1.53 M $BMPyrVOF_4$ (liquid), and (c) BMPyrTFSA (liquid).

Figure 7 Cyclic voltammograms of a Pt electrode in BMPyrTFSA containing 17.0 mM of $BMPyrVOF_4$ at 298 K. Scan rate: (a) 0.1, (b) 0.5, (c) 1, (d) 2, (e) 5, (f) 10, and (g) 20 mV s^{-1}.

Figure 8 The $\ln v^{1/2} - E_p^c$ plots for the reduction of VOF_4^- in BMPyrTFSA containing 17.0 mM of $BMPyrVOF_4$.

Figure 9 The $v^{1/2} - i_p^c$ plots for the reduction of VOF_4^- in BMPyrTFSA containing 17.0 mM of $BMPyrVOF_4$.

Figure 10 The $t^{-1/2} - i$ plots for the reduction of VOF_4^- in BMPyrTFSA containing 17.0 mM of $BMPyrVOF_4$.

Figure 1

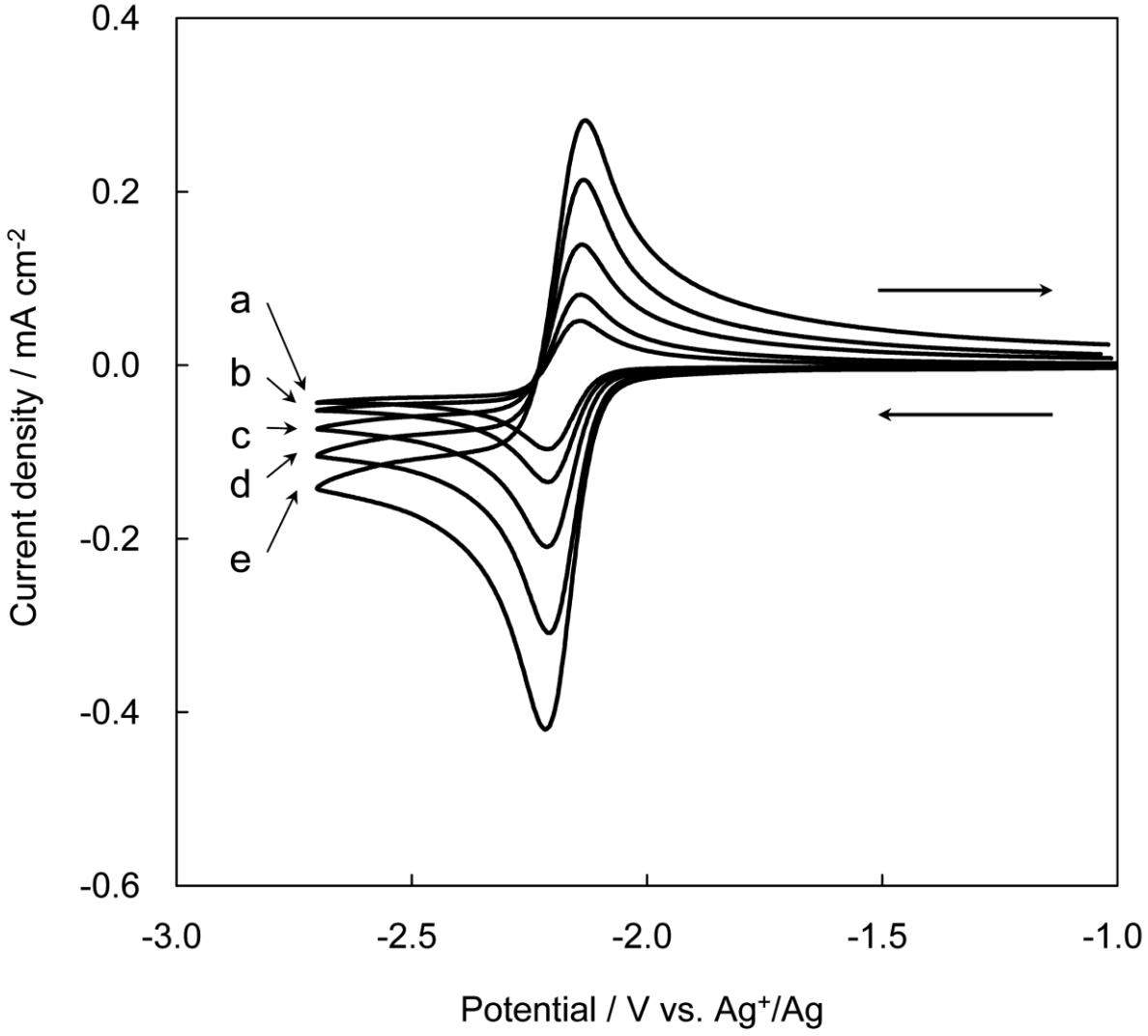
0.4
0.2
0.0
-0.2
-0.4
-0.6
-3.0
-2.5
-2.0
-1.5
-1.0
Current density / mA cm-2
Potential / V vs. Ag+/Ag
a
b
c
d
e

Figure 2

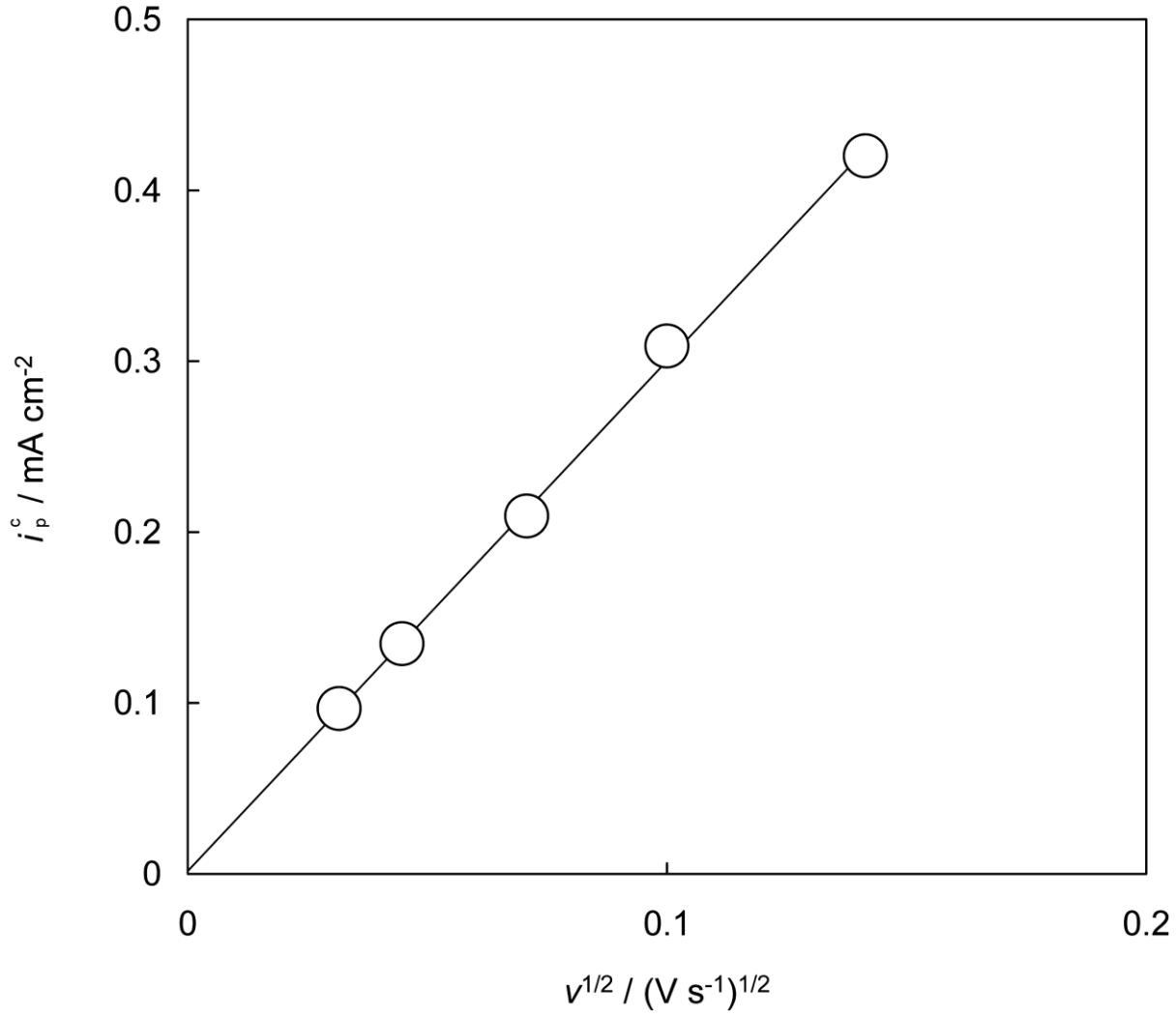

Figure 3

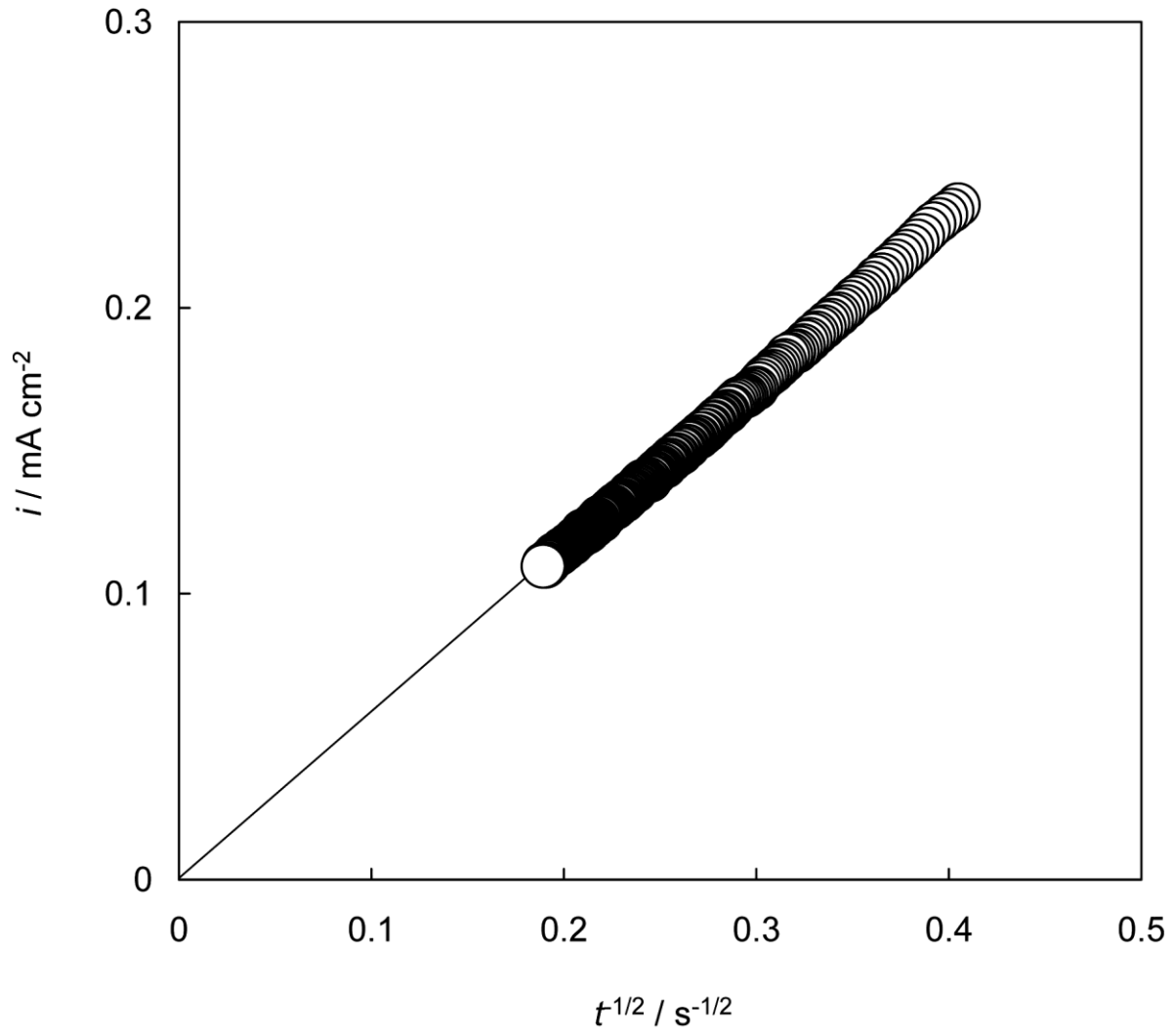

Figure 4

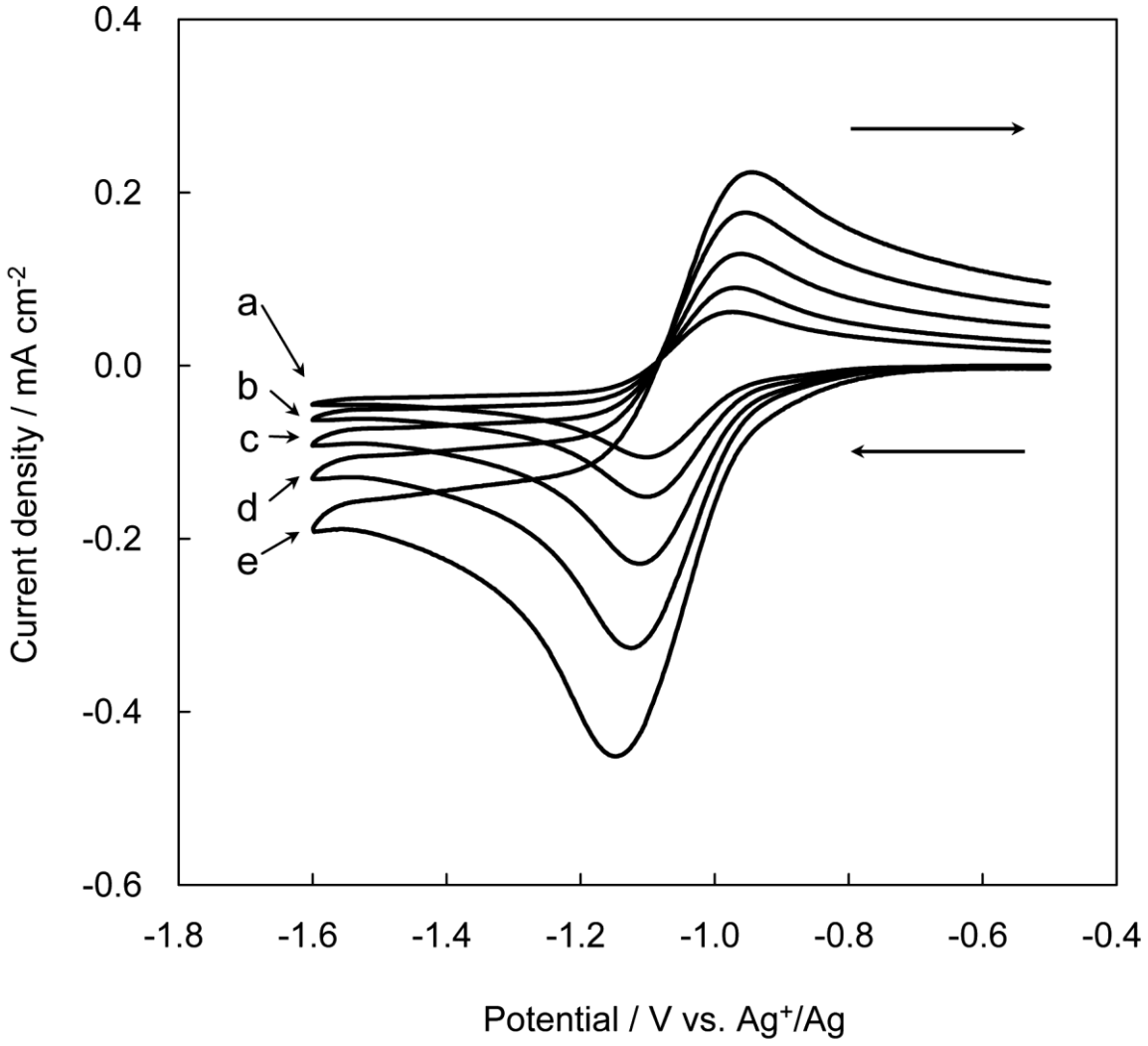
0.4
0.2
0.0
-0.2
-0.4
-0.6
-1.8
-1.6
-1.4
-1.2
-1.0
-0.8
-0.6
-0.4
Current density / mA cm-2
Potential / V vs. Ag+/Ag
a
b
c
d
e

Figure 5

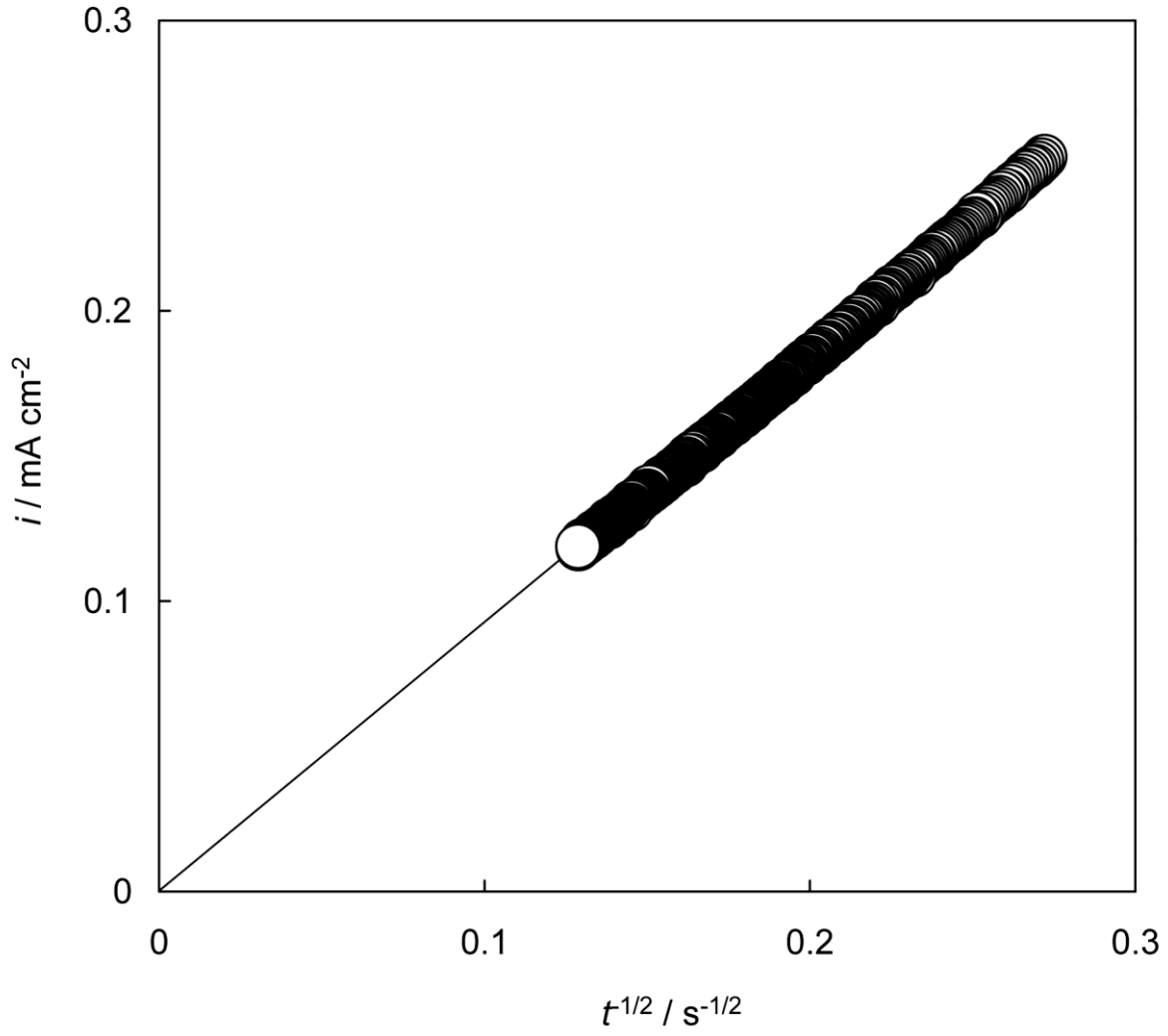

Figure 6

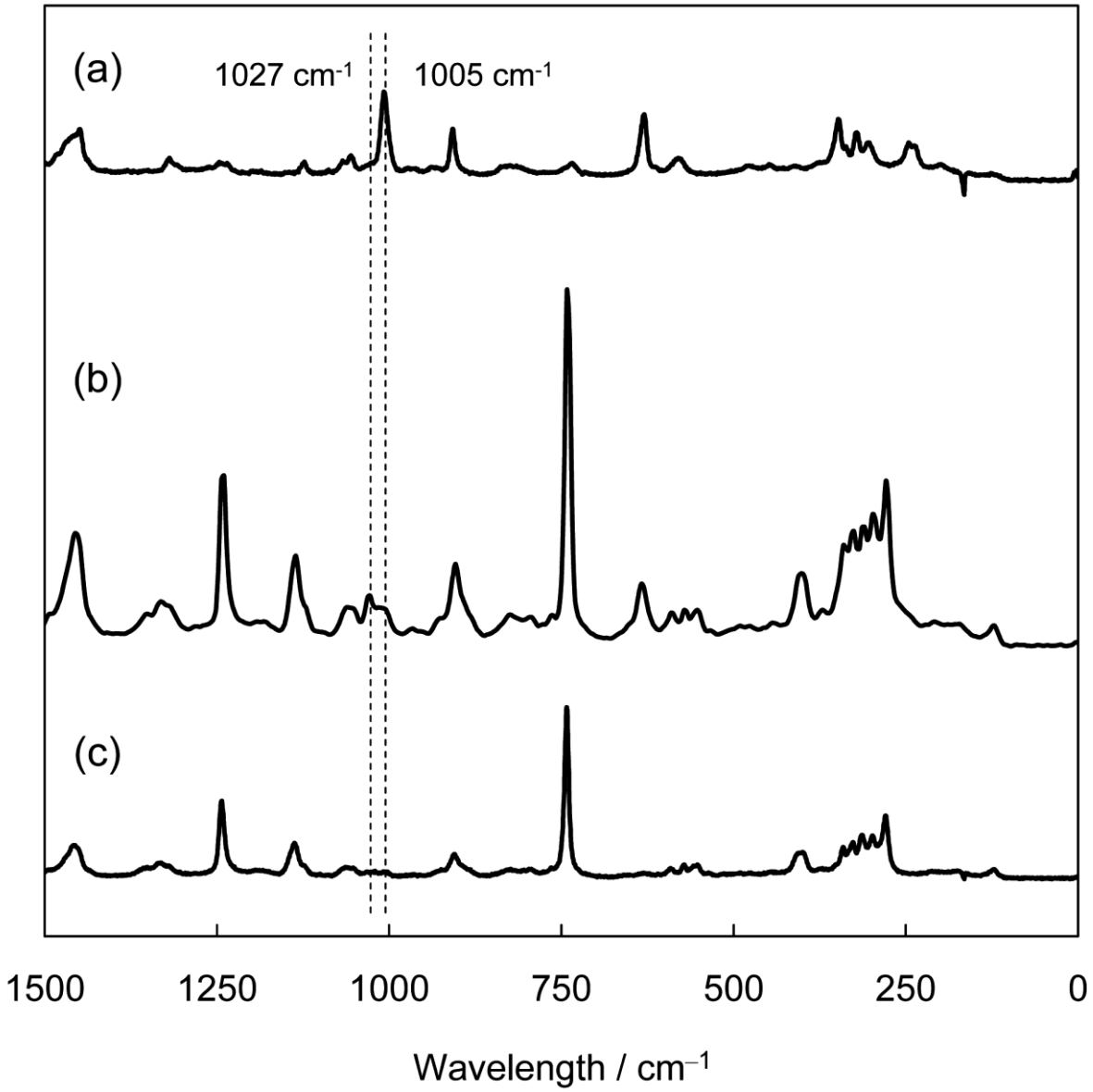
(a)
1027 cm-1
1005 cm-1
(b)
(c)
1500
1250
1000
750
500
250
0
Wavelength / cm−1

Figure 7

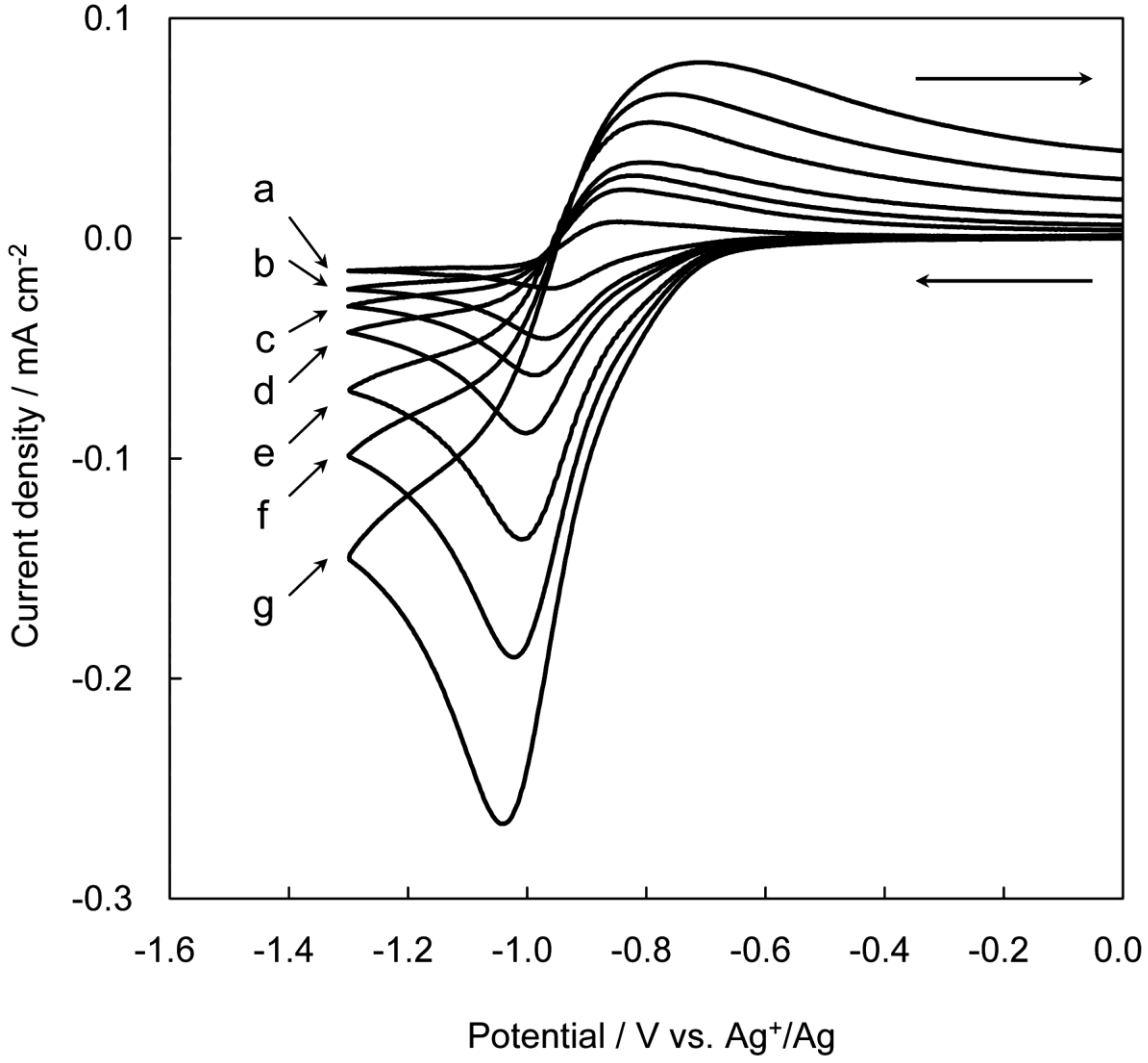
0.1
0.0
-0.1
-0.2
-0.3
Current density / mA cm-2
a
b
c
d
e
f
g
-1.6
-1.4
-1.2
-1.0
-0.8
-0.6
-0.4
-0.2
0.0
Potential / V vs. Ag+/Ag

Figure 8

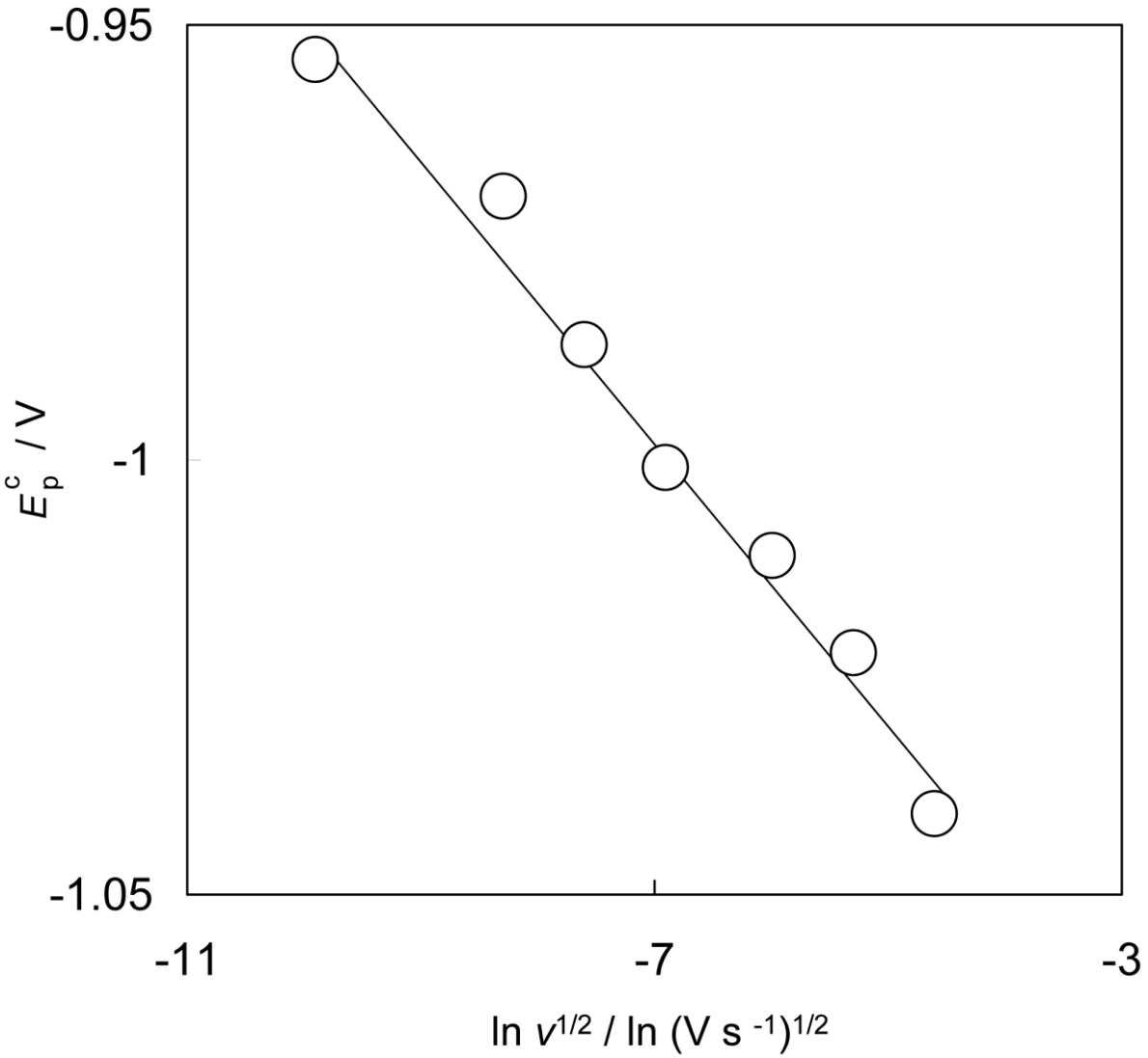

Figure 9

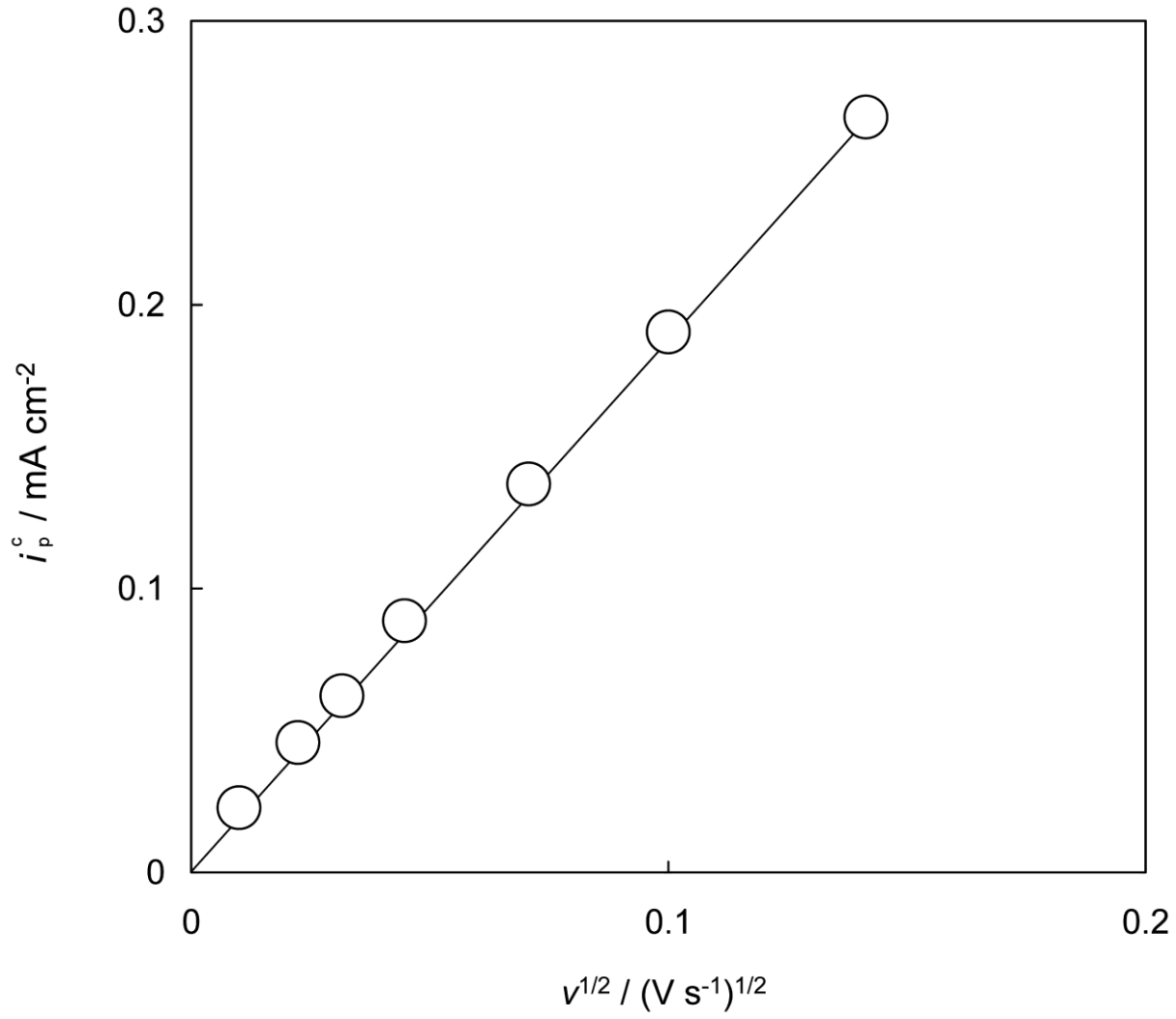

Figure 10

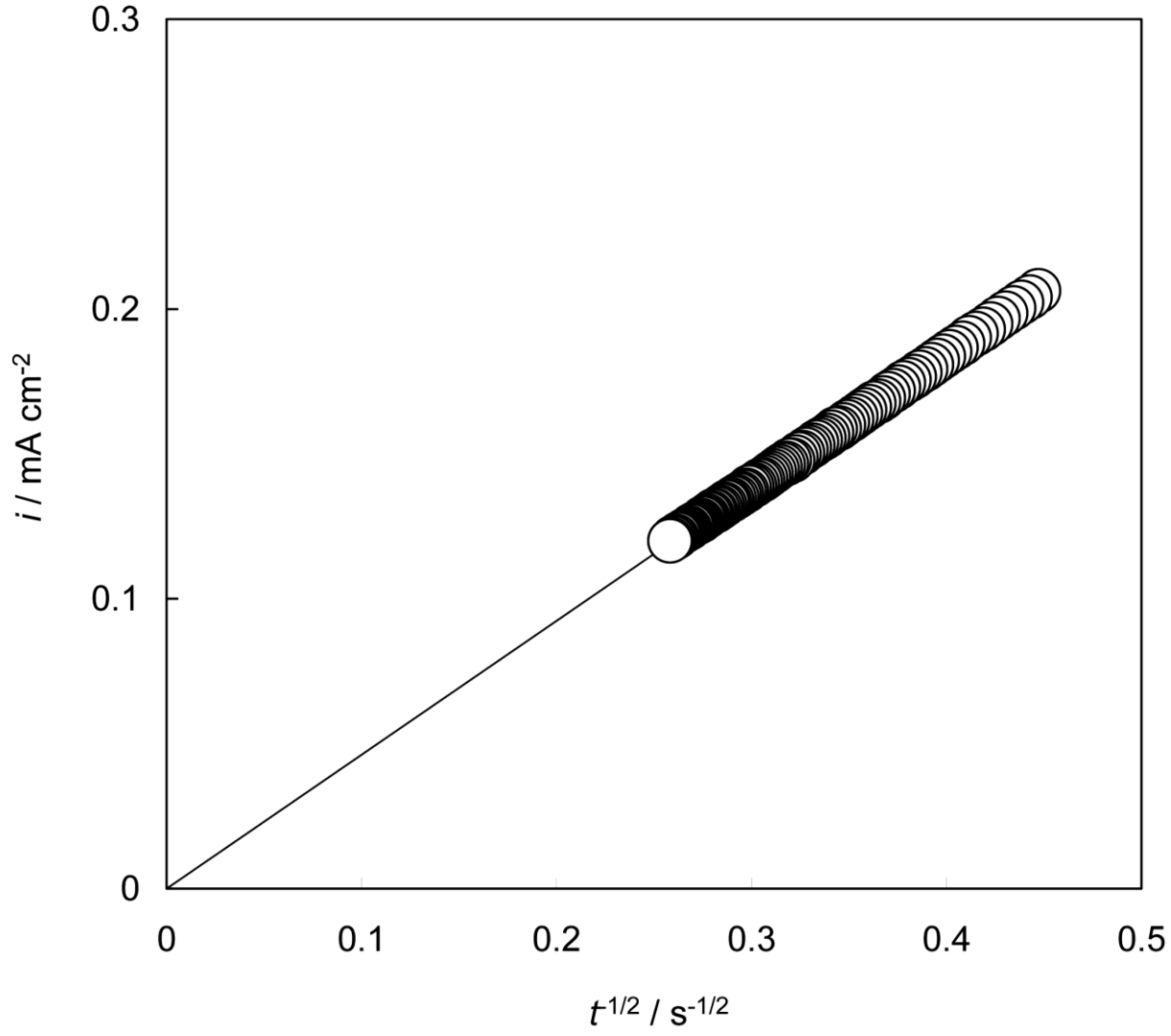

Graphical Abstract